ACS chemical biology

Articles

pubs.acs.org/acschemicalbiology

Quasithermodynamic Contributions to the Fluctuations of a Protein Nanopore

Belete R. Cheneke,[†] Bert van den Berg,[‡] and Liviu Movileanu*[,†,§,∥]

[†]Department of Physics, Syracuse University, 201 Physics Building, Syracuse, New York 13244-1130, United States

[‡]Institute for Cellular and Molecular Biosciences, Newcastle University, Newcastle upon Tyne, NE2 4HH, United Kingdom

[§]Structural Biology, Biochemistry, and Biophysics Program, Syracuse University, 111 College Place, Syracuse, New York 13244-4100, United States

[∥]Syracuse Biomaterials Institute, Syracuse University, 121 Link Hall, Syracuse, New York 13244, United States

Supporting Information

ABSTRACT: Proteins undergo thermally activated conformational fluctuations among two or more substates, but a quantitative inquiry on their kinetics is persistently challenged by numerous factors, including the complexity and dynamics of various interactions, along with the inability to detect functional substates within a resolvable time scale. Here, we analyzed in detail the current fluctuations of a monomeric β-barrel protein nanopore of known high-resolution X-ray crystal structure. We demonstrated that targeted perturbations of the protein nanopore system, in the form of loop-deletion mutagenesis, accompanying alterations of electrostatic interactions between long extracellular loops, produced modest changes of the differential activation free energies calculated at 25 °C, $\Delta\Delta G^{\ddagger}$, in the range near the thermal energy but substantial and correlated modifications of the differential activation enthalpies, $\Delta\Delta H^{\ddagger}$, and entropies, $\Delta\Delta S^{\ddagger}$. This finding indicates that the local conformational reorganizations of the packing and flexibility of the fluctuating loops lining the central constriction of this protein nanopore were supplemented by changes in the single-channel kinetics. These changes were reflected in the enthalpy−entropy reconversions of the interactions between the loop partners with a compensating temperature, T_C, of ∼300 K, and an activation free energy constant of ∼41 kJ/mol. We also determined that temperature has a much greater effect on the energetics of the equilibrium gating fluctuations of a protein nanopore than other environmental parameters, such as the ionic strength of the aqueous phase as well as the applied transmembrane potential, likely due to ample changes in the solvation activation enthalpies. There is no fundamental limitation for applying this approach to other complex, multistate membrane protein systems. Therefore, this methodology has major implications in the area of membrane protein design and dynamics, primarily by revealing a better quantitative assessment on the equilibrium transitions among multiple well-defined and functionally distinct substates of protein channels and pores.

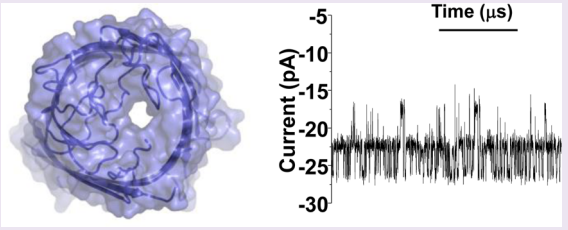

β-barrel membrane protein channels and pores often fluctuate around a most probable equilibrium substate. On some occasions, such conformational fluctuations can be detected by high-resolution, time-resolved, single-channel electrical recordings.[1−6] In principle, this is possible due to reversible transitions of a β-barrel protein between a conductive and a less conductive substate, resulting from a local conformational modification occurring within its lumen, such as a transient displacement of a more flexible polypeptide loop or even a movement of a charged residue.[7,8] In general, such fluctuations result from a complex combination and dynamics of multiple interactions among various parts of the same protein.[9,10] The underlying processes by which β-barrel membrane proteins undergo a discrete switch among various functionally distinct energetic substates with different levels of ionic conductance are elusive.[11] Two possible postulations were raised for the mechanisms of discrete fluctuations in β-barrel channels and pores: (i) an electrostatic process driven by the local electric field changes within the central constriction of the β-barrel lumen, occluding the permeation pathway for ions,[12,13] and (ii) the steric mechanism that implies substantial movements of the long occluding loops, generating dynamic translocation barriers of the protein lumen.[5,6,14]

Here, we examined in detail the mechanism of the thermally activated current fluctuations of OccK1 (Figure 1),[15] a weakly anion-selective, monomeric β-barrel protein that is the archetype of the outer membrane carboxylate channel (Occ) family of *Pseudomonas aeruginosa* (Supporting Information, Figures S1−S3).[15−18] Pseudomonads utilize specialized conductive pathways, such as the members of the Occ protein family, to facilitate the import of water-soluble, low-molecular weight nutrients required for the growth and function of the cell.[19,20] The high-resolution, X-ray crystal structure of OccK1

Received: October 6, 2014
Accepted: December 5, 2014
Published: December 5, 2014

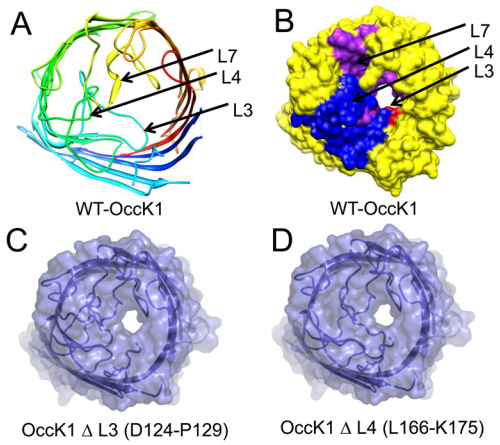

Figure 1. Cross-sectional view of the wild-type OccK1 (WT-OccK1) protein, illustrating loops L3, L4, and L7. (A) A top view of WT-OccK1. (B) A top view of the molecular surface of WT-OccK1. (C) A top view of the molecular surface of OccK1 ΔL3. (D) A top view of the molecular surface of OccK1 ΔL4. WT-OccK1, OccK1 ΔL3, and OccK1 ΔL4 show a closely similar central constriction of the open pore.

reveals a kidney-shaped structure of the nanopore lumen. The major extracellular loops L3, L4, and L7 line the central constriction of the pore lumen (Figure 1; Supporting Information, Table S1), which measures about 5 Å in diameter.[21]

The advantages of this nanopore for the exploration of the quasithermodynamic contributions to protein fluctuations include the following: (i) The high-resolution, X-ray crystal structure of the OccK1 protein is now available,[15,21] permitting rationally designed modifications of the fluctuating regions (e.g., the extracellular loops). (ii) The β-barrel scaffold features a very high thermodynamic stability, which is determined by the contribution of a large network of hydrogen bonds among antiparallel β strands. Protein engineering within a localized region of the very flexible loop domains is expected to produce a well-correlated change in the dynamics of the current fluctuations, but without the conformational alteration in the packing and stability of the β-barrel scaffold.[22−26] (iii) The single-channel electrical signature of the OccK1 protein shows three distinguishable and time-resolvable open substates, whose biophysical features were previously examined in detail.[27] The unitary conductance of the OccK1 protein is ∼310 pS in 1 M KCl.[17,21] (iv) The single-channel kinetics comprised of well-defined, functionally distinct conductance substates only reflect the fluctuating loop-based domains within the nanopore lumen.[5,7,8,28,29] (v) OccK1 is a monomeric protein, eliminating complexity of gating events produced by individual protomers of the oligomeric structure of membrane proteins, such as those encountered with the outer membrane proteins F (OmpF)[30,31] and C (OmpC).[32]

In this work, we employed single-molecule electrophysiology measurements to examine the gating fluctuations of the OccK1 protein nanopore among three distinguishable open substates (Figure 2). Such analysis has indeed required a systematic change of temperature for revealing the kinetic and energetic contributions to these conformational fluctuations. Our experimental strategy was to produce a small perturbation of the protein nanopore system (e.g., a deletion mutant of a flexible region of the pore lumen), which kept the equilibrium transitions among the same number of open substates, but it

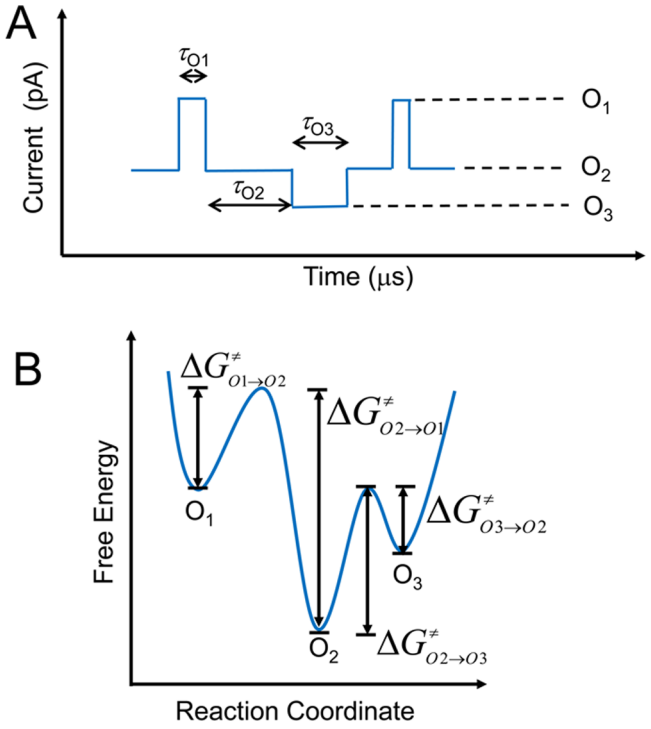

Figure 2. Cartoon presenting a three-open substate fluctuating system. (A) A model of a single-channel current recording of a fluctuating protein nanopore inserted into a planar lipid membrane. The current fluctuations occurred among O_1, O_2, and O_3, which were three open substates. (B) A free energy landscape model illustrating the kinetic transitions among the three open substates. This model shows the activation free energies characterizing various kinetic transitions ($\Delta G_{O1\rightarrow O2}{}^{\ddagger}$, $\Delta G_{O2\rightarrow O1}{}^{\ddagger}$, $\Delta G_{O1\rightarrow O3}{}^{\ddagger}$, and $\Delta G_{O3\rightarrow O1}{}^{\ddagger}$).

produced a detectable redistribution among the open substates.[11] This redistribution also required major alterations in the ionic flow, so that a detectable change in the duration and frequency of the gating events was readily observable. Of course, such perturbation should not have resulted in an observable modification of the number of energetic substates, producing far-from-equilibrium dynamics of the protein nanopore. Otherwise, meaningful comparisons of the system response and adaptation under various experimental contexts were not possible. Therefore, we inspected such protein modifications within the most flexible region of the nanopore lumen, with a focus on the large extracellular loops lining the central constriction. This molecular modeling investigation revealed that targeted loop deletions in L3 and L4 can be accomplished without a far-from-equilibrium perturbation of the protein nanopore.

Here, we hypothesized that the energetic impact of major electrostatic interactions among the loops is accompanied by local structural changes producing an alteration of the single-channel kinetics. Using determinations of the duration of open substates (Figure 2), we were able to extract kinetic rate constants and equilibrium constants for various detectable transitions. Such an approach permitted the calculation of quasithermodynamic ($\Delta H^{\ddagger}$, $\Delta S^{\ddagger}$, $\Delta G^{\ddagger}$) and standard thermodynamic (ΔH°, ΔS°, ΔG°) parameters characterizing these transient gating fluctuations. $\Delta H^{\ddagger}$, $\Delta S^{\ddagger}$, and $\Delta G^{\ddagger}$ denote the quasithermodynamic parameters of the equilibrium between a ground state and a transition state, at which point the protein nanopore is thermally activated. A systematic analysis of these

dx.doi.org/10.1021/cb5008025 | ACS Chem. Biol. 2015, 10, 784−794

parameters determined for loop-deletion OccK1 mutants enabled the identification of significant changes of the differential activation enthalpies and entropies but modest modifications of the differential transition free energies. Although the protein nanopore analyzed in this work is pertinent to a three-open substate system, we anticipate no technical problems or fundamental limitations for expanding this methodology to other multiopen substate membrane protein channels or pores, whose quasithermodynamic values can provide a more quantitative and mechanistic understanding on their equilibrium transitions.

RESULTS

Strategy for Designing Loop-Deletion Mutants of OccK1. A primary objective of this work was the examination of the current fluctuations produced by large extracellular loops when a small number of stabilizing electrostatic interactions were removed. To accomplish this, we explored the high-resolution X-ray crystal structure of the OccK1 protein nanopore.[21] We determined that L3, L4, and L7 are the primary channel-occluding extracellular loops. In order to achieve these loop deletions, we selected sites in which the residues immediately before and after the deletion are in close proximity, so that they can be linked via a single glycine residue. In this way, we avoided significant conformational alterations of the β-barrel scaffold. Even if this strategy was met, we discovered that the removal of strong electrostatic interactions between the mutated loop and other loops produced dramatic changes in the single-channel electrical signature of the loop-deletion OccK1 mutant as compared to the wild-type OccK1 (WT-OccK1) protein. For example, in the preliminary stage of this work, we produced a loop-deletion OccK1 ΔL7 mutant, whose deleted residues S281-G287 include a critical intramolecular R284-D116 salt bridge positioned between loops L7 and L3. High-resolution X-ray crystal structure of OccK1 also reveals a large extent of L7 lining the central constriction of the nanopore lumen (Figure 1A,B).[21] Deletion of these residues not only results in an apparent expansion of the cross-sectional area of the central constriction but also induces possible destabilization among the contacts between L3 and L7. Indeed, the high-resolution, single-channel recordings acquired with OccK1 ΔL7 revealed a ∼2-fold increase in the unitary conductance accompanied by a very noisy electrical signature, which was comprised of highly frequent and short-lived current spikes.[27] Such a finding provided two pieces of information: (i) L7 lines the central constriction, and (ii) OccK1 ΔL7 undergoes a major alteration of the tight loop packing characterized by its contacts with loop L3.

After loop-deletion OccK1 mutants were produced, it was important to identify closely similar single-channel electrical signatures consisting of three open substates, among which the protein undergoes discrete and detectable functional transitions. This has been accomplished with two distinct loop-deletion mutants, OccK1 ΔL3 (D124-P129) and OccK1 ΔL4 (L166-K175) (Supporting Information, Table S2).[27] It should be emphasized that OccK1 ΔL3 lacks a critical D124-R16 salt bridge positioned between loop L3 and the pore wall (PW). This loop-deletion OccK1 ΔL3 mutant also lacks a number of hydrogen bonds, such as G125 bb (L3)−Y18 sc (PW), R126 sc (L3)−R16 sc (PW), and R126 sc (L3)−N76 sc (L2). In addition, OccK1 ΔL3 lacks several hydrophobic and van der Waals interactions, primarily involving L127 (L3)−P129 (L3). On the contrary, OccK1 ΔL4 does not lack any strong ion-pair interaction but removes several hydrogen bonds and van der Waals interactions between L4 and L6, L4 and L7, and L4 and PW (Supporting Information, Table S2). Because only a glycine residue was added between the residues just before and after deletion, these loop deletions were not expected to alter the average structure of the β-barrel scaffold.

WT-OccK1 and Loop-Deletion OccK1 ΔL3 and OccK1 ΔL4 Mutants Exhibit Three-Open Substate Kinetics. Temperature-dependent, single-channel electrical recordings were accomplished using an elevated KCl concentration to maximize the signal-to-noise ratio (Methods; Supporting Information, Table S3, Figure S4). Thus, in 2 M KCl, the unitary conductance of the OccK1 protein nanopore is ∼550 pS. As an example, Figure 3 illustrates single-channel electrical traces acquired with the WT-OccK1 protein nanopore in 2 M KCl and 10 mM potassium phosphate, pH 7.4, at a temperature of 20 °C and at a transmembrane potential of −40 mV. Here, O_1, O_2, and O_3 denote the open substates featuring the low, medium, and high current amplitudes, respectively. The time constants τ_1, τ_2, and τ_3, which correspond to the average duration of the open substates O_1, O_2, and O_3, respectively, were derived from standard dwell time histograms (Figure 3). The fits of the data were accomplished using log likelihood ratio (LLR) tests to compare various fitting models.[33−35] In general, the fit of the dwell time histograms contained a well-

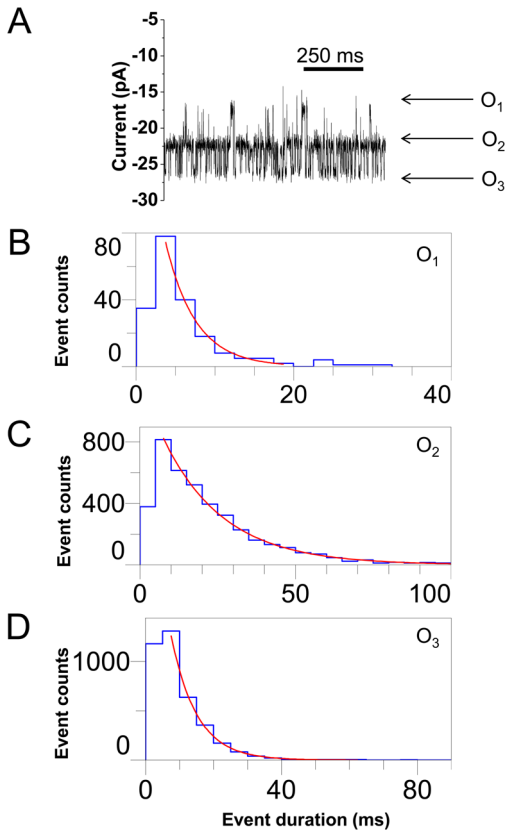

Figure 3. A single-channel trace obtained with WT-OccK1 at a transmembrane potential of −40 mV. (A) A typical trace; standard duration histograms of the O_1, O_2, and O_3 events are illustrated in panels C, D, and E, respectively. The results of the fits were the following: (B) τ_{O1} = 4.6 ± 0.4 ms; (C) τ_{O2} = 19.5 ± 0.4 ms; (D) τ_{O3} = 7.5 ± 0.2 ms. The buffer solution was 2 M KCl and 10 mM potassium phosphate, pH 7.4. The temperature in the chamber was 20 °C. The single-channel electrical trace was filtered at 0.5 kHz.

dx.doi.org/10.1021/cb5008025 | ACS Chem. Biol. 2015, 10, 784−794

defined single-exponential function, as determined by the LLR test value. Deviations from single-exponential distributions of the event durations were noticed in a few situations. Such imperfections of single-exponential time distributions were likely caused by hidden, or undetectable, conformational substates in the biomolecular system and not by limited time resolution of the instrumentation. In such instances, we used averages of the detected event dwell times. Using the rise time of the low-pass Bessel filter $T_r = 339/F_c$,[36,37] where T_r and F_c are the rise time and corner frequency, respectively, we can obtain the dead time $T_d = 0.54 \times T_r$. For a value of the corner frequency F_c = 500 Hz, we derive T_r = ~680 μs, so that T_d = 367 μs. In this work, most current transitions were longer than 0.4 ms. We calculated that the missed current blockades, under all experimental conditions explored in this study, were not more than 8% of the total number of events in each recorded single-channel electrical trace.[33,34,38] For example, the average dwell times determined by standard event duration histograms were always greater than 1 ms. Therefore, additional corrections for missed events were not necessary.[33,38]

A detailed analysis of the expanded single-channel electrical traces showed that there is a reversible transition between O_1 and O_2, and O_2 and O_3 substates, but no O_1 to O_3 or O_3 to O_1 transition was observed. Hence, we developed a kinetic scheme model, which fits to three minima of free energy landscape (Figure 2). It is worth mentioning that the number of open substates observed with WT-OccK1 and loop-deletion OccK1 ΔL3 and OccK1 ΔL4 mutants is always preserved in the temperature range inspected in this work (0−25 °C). For example, Figure 4 shows the single-channel electrical traces acquired with the OccK1 protein nanopore at temperatures of 1, 8, and 22 °C. At elevated temperatures, the frequency of the O_2 and O_3 events increased, whereas their duration decreased, which is in accord with a reduction in the activation free energies corresponding to the $O_2 \rightarrow O_3$ and $O_3 \rightarrow O_2$ current transitions. In addition, the unitary conductance increased owing to the temperature-induced modification of the conductivity of ionic solution in the chamber.

The four rate constants underlying the kinetics of the gating fluctuations observed with OccK1, OccK1 ΔL3, and OccK1 ΔL4, $k_{O1\rightarrow O2}$, $k_{O2\rightarrow O1}$, $k_{O2\rightarrow O3}$, and $k_{O3\rightarrow O2}$, can be calculated using the duration and frequencies of the O_1 and O_3 events. Using a chemical kinetics formalism for single-molecule fluctuations of OccK1,[39] we formulate the following system of partial differential equations:[40]

$$\begin{aligned}
\frac{dP_{O1}}{dt} &= -k_{O1\rightarrow O2}P_{O1} + k_{O2\rightarrow O1}P_{O2} \\
\frac{dP_{O2}}{dt} &= +k_{O1\rightarrow O2}P_{O1} - k_{O2\rightarrow O1}P_{O2} + k_{O3\rightarrow O2}P_{O3} \\
&\quad - k_{O2\rightarrow O3}P_{O2} \\
\frac{dP_{O3}}{dt} &= -k_{O3\rightarrow O2}P_{O3} + k_{O2\rightarrow O3}P_{O2}
\end{aligned} \tag{1}$$

where P_{O1}, P_{O2}, and P_{O3} indicate the occupancy probabilities of the O_1, O_2, and O_3 substates, respectively. Here, we define the three occupancy probabilities using the following expressions:

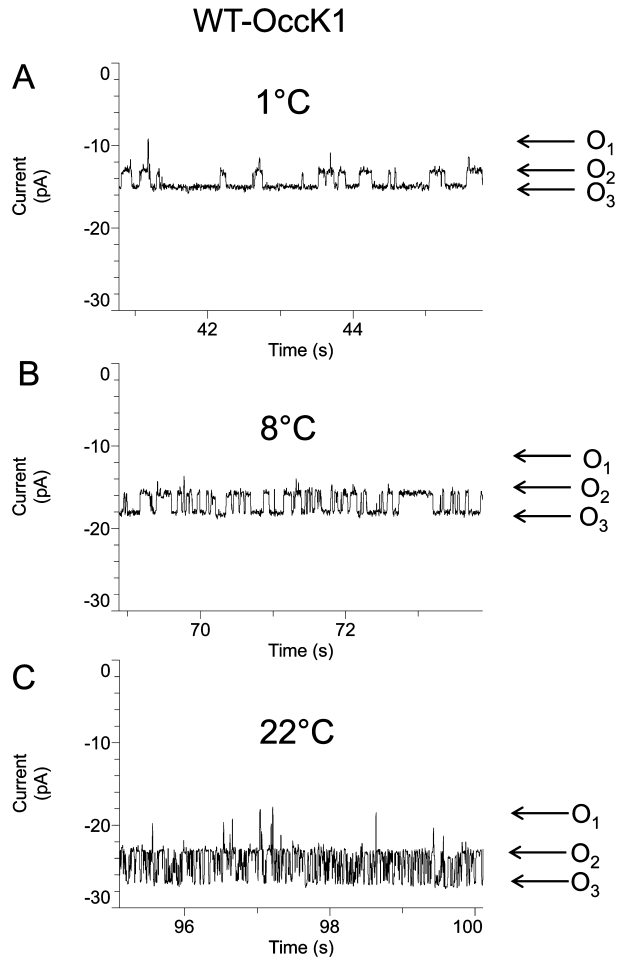

Figure 4. Representative single-channel electrical traces collected with WT-OccK1 at various temperatures. Other conditions are similar to those presented in the legend of Figure 3.

$$\begin{aligned}
P_{O1} &= \frac{T_{O1}}{T} = \frac{N_{O1}\tau_{O1}}{T} = F_{O1}\tau_{O1} \\
P_{O2} &= \frac{T_{O2}}{T} = \frac{N_{O2}\tau_{O2}}{T} = (F_{O1} + F_{O3})\tau_{O2} \\
P_{O3} &= \frac{T_{O3}}{T} = \frac{N_{O3}\tau_{O3}}{T} = F_{O3}\tau_{O3}
\end{aligned} \tag{2}$$

where T_{O1}, T_{O2}, and T_{O3} denote the total occupied times by the O_1, O_2, and O_3 substates, respectively. N_{O1}, N_{O2}, and N_{O3} represent the total number of events recorded in the O_1, O_2, and O_3 substates, respectively, whereas T is the total time of recording. F and τ are the frequency and average duration of events corresponding to an open substate, respectively. The kinetic rate constants for reaching the O_1 and O_3 substates are given by the corresponding frequencies of events and are normalized to P_{O2}:

$$\begin{aligned}
k_{O2\rightarrow O1} &= \frac{F_{O1}}{P_{O2}} = \frac{F_{O1}}{1 - (F_{O1}\tau_{O1} + F_{O3}\tau_{O3})} \\
k_{O2\rightarrow O3} &= \frac{F_{O3}}{P_{O2}} = \frac{F_{O3}}{1 - (F_{O1}\tau_{O1} + F_{O3}\tau_{O3})}
\end{aligned} \tag{3}$$

Because the event probabilities are constant at equilibrium, the partial derivatives of eqs 1 are zero. Therefore,

dx.doi.org/10.1021/cb5008025 | ACS Chem. Biol. 2015, 10, 784−794

$$k_{O1\rightarrow O2} = \frac{1}{\tau_{O1}}$$

$$k_{O3\rightarrow O2} = \frac{1}{\tau_{O3}} \quad (4)$$

These calculations show that the four kinetic rates can be determined using the frequencies of events and average durations of the flanked O_1 and O_3 open substates.

Determination of the Enthalpic and Entropic Contributions to the Fluctuations of a Protein Nanopore Using Arrhenius' Formalism. In Figure 5, we present the

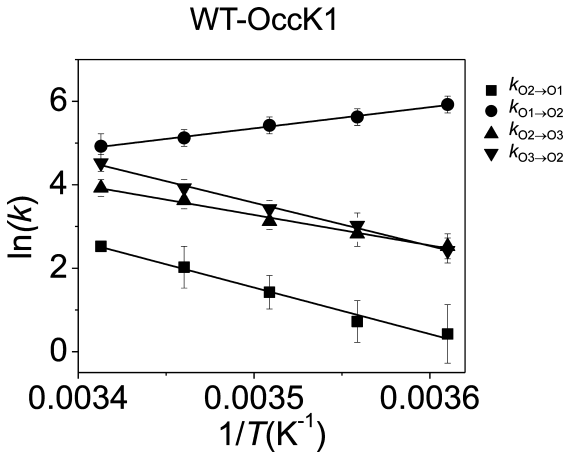

Figure 5. Arrhenius plot of the kinetic rate constants characterizing four distinct current fluctuations observed in WT-OccK1. Other conditions are similar to those presented in the legend of Figure 3.

logarithmic dependence of the four kinetic rate constants on the inverse absolute temperature. The data were acquired at an applied transmembrane voltage of −40 mV. All rate constants, k, satisfy the Arrhenius equation:

$$k = k_0 \exp\left[-\frac{\Delta G^{\ddagger}}{RT}\right] \quad (5)$$

where k_0 is a barrier-free rate parameter that depends on each biomolecular system according to Kramers' theory,[41] whereas $\Delta G^{\ddagger}$ denotes the activation free energy. Here, R and T indicate the universal gas constant and absolute temperature, respectively. We have used this equation to extract the quasithermodynamic parameters of all open substates, along with the standard definition of $\Delta G^{\ddagger}$:

$$\Delta G^{\ddagger} = \Delta H^{\ddagger} - T\Delta S^{\ddagger} \quad (6)$$

where $\Delta H^{\ddagger}$ and $\Delta S^{\ddagger}$ are the activation enthalpy and entropy, respectively. All kinetic rate constants follow a linearized Arrhenius equation:

$$\ln k = -\frac{\Delta H^{\ddagger}}{RT} + \phi(k_0) \quad (7)$$

where

$$\phi(k_0) = \ln k_0 + \frac{\Delta S^{\ddagger}}{R} \quad (8)$$

is a term that is independent of temperature. Using the slope of eq 7, we were able to obtain values for $\Delta H^{\ddagger}$ corresponding to each rate constant. It is important to note that these values are independent of the barrier-free rate parameter. However, we had to assume the value of k_0 to estimate the entropic contribution to the activation free energy corresponding to each transition. For the activation entropies and activation free energies, we used $k_0 = 10^9$ s^{-1}, which approximates the frequency of diffusional transitions over a path distance of ∼1 nm.[42] This assumption will be canceled out in the case of differential activation entropies ($\Delta\Delta S^{\ddagger}$) and free energies ($\Delta\Delta G^{\ddagger}$) (the Discussion section). Using the above-mentioned fits, we noticed that three of the rate constants, i.e., $k_{O2\rightarrow O1}$, $k_{O2\rightarrow O3}$, and $k_{O3\rightarrow O2}$, have positive values of $\Delta H^{\ddagger}$ (Figure 5). In contrast, the rate constant $k_{O1\rightarrow O2}$ has a negative contribution of $\Delta H^{\ddagger}$. This result is because the slopes of the dependence of $k_{O2\rightarrow O1}$, $k_{O2\rightarrow O3}$, and $k_{O3\rightarrow O2}$ on $1/T$ are negative. According to eq 7, a negative slope would mean a positive value of $\Delta H^{\ddagger}$. Vice versa, $\Delta H^{\ddagger}$ is negative.

The Compensation Effect of the Activation Entropies and Enthalpies of All Kinetic Rate Constants. In Figure 6, we presented the plot of all data points of $\Delta H^{\ddagger}$ versus $\Delta S^{\ddagger}$ determined for WT-OccK1, OccK1 ΔL3, and OccK1 ΔL4, and at applied transmembrane potentials of +40 and −40 mV. The $O_1 \rightarrow O_2$ transition is accompanied by a negative activation enthalpy. The compensation nature of $\Delta H^{\ddagger}$ and $\Delta S^{\ddagger}$ values is illustrated by their closely linear relationship.[43−45] $\Delta H^{\ddagger}$ values corresponding to the $O_2 \rightarrow O_3$ transition are positive but smaller than those corresponding to the $O_2 \rightarrow O_1$ and $O_3 \rightarrow O_2$ transitions. A linear regression of the form $\Delta H^{\ddagger} = \Delta G^{\ddagger} + T\Delta S^{\ddagger}$ was performed, providing a compensation temperature T_c of ∼300 K and an activation free energy constant $\Delta G_c^{\ddagger}$ of ∼40.5 kJ/mol. The value of $\Delta G_c^{\ddagger}$ was extracted from the intercept of the plot with the vertical $\Delta H^{\ddagger}$ axis. $\Delta G_c^{\ddagger}$ is comparable with the average $\Delta G^{\ddagger}$ of all open substates at 25 °C (∼41 kJ/mol; Supporting Information, Table S4).

Determination of the Equilibrium Entropies, Enthalpies, and Free Energies. In Figure 7, we show the plot of the equilibrium enthalpy ΔH° versus equilibrium entropy ΔS° for WT-OccK1, OccK1 ΔL3, and OccK1 ΔL4. These thermodynamic parameters were determined from the ratio of the kinetic rate constants participating in that respective reversible transition:[46]

$$\Delta G^{\circ}_{O1\rightarrow O2} = \ln\left(\frac{k_{O1\rightarrow O2}}{k_{O2\rightarrow O1}}\right)$$

$$\Delta G^{\circ}_{O3\rightarrow O2} = \ln\left(\frac{k_{O3\rightarrow O2}}{k_{O2\rightarrow O3}}\right) \quad (9)$$

where

$$\Delta G^{\circ} = \Delta H^{\circ} - T\Delta S^{\circ} \quad (10)$$

A linear regression of $\Delta H^{\circ} = \Delta G^{\circ} + T_c\Delta S^{\circ}$ was performed (Figure 7), enabling the determination of a compensation temperature $T_c = 299 \pm 2$ K. In addition, we calculated the weighted average of standard free energy $\Delta G^{\circ} = -2.31 \pm 0.58$ kJ/mol. Therefore, we can rewrite eq 10 as follows:

$$\Delta H^{\circ} - (299 \pm 2\ \mathrm{K})\Delta S^{\circ} = -2.31 \pm 0.58\ \mathrm{kJ/mol} \quad (11)$$

which defines the quantitative linear relationship between ΔH° and ΔS° obtained with this system.

Dependence of the Equilibrium Free Energies on Temperature Reveals Two Distinct Reversible Current Fluctuations. Finally, we were interested to determine the dependence of the equilibrium free energies corresponding to

dx.doi.org/10.1021/cb5008025 | ACS Chem. Biol. 2015, 10, 784−794

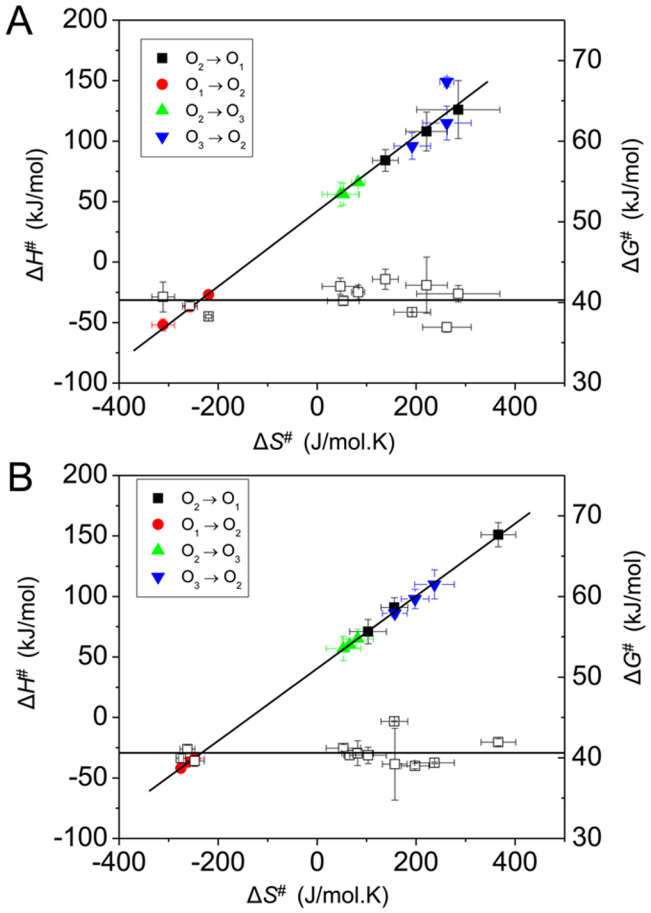

Figure 6. Activation free entropy versus activation free enthalpy of WT-OccK1 and its deletion mutants. (A) The transmembrane potential was +40 mV. The compensation temperature, T_c, was 303 ± 3 K. The activation free energy constant, $\Delta G_c^{\#}$, was 40.5 ± 0.5 kJ/mol. The right axis shows the activation free energy, $\Delta G^{\#}$, which was calculated at a temperature of 25 °C (open squares). The horizontal line is the weighted average of the activation free energy, $\Delta G^{\#}$ = 40.3 kJ/mol, which was determined at 25 °C. (B) The transmembrane potential was −40 mV. The compensation temperature, T_c, was 299 ± 2 K. The activation free energy constant, $\Delta G_c^{\#}$, was 40.6 ± 0.5 kJ/mol. The right axis shows the activation free energy, $\Delta G^{\#}$, which was calculated at a temperature of 25 °C (open squares). The horizontal line is the weighted average of the activation free energy, $\Delta G^{\#}$=40.6 kJ/mol, which was determined at 25 °C. Other conditions are similar to those presented in the legend of Figure 3.

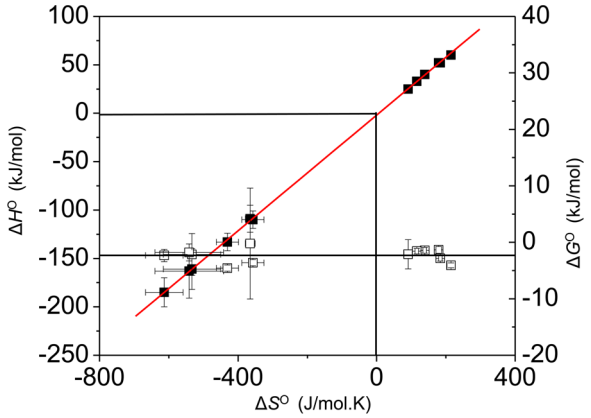

Figure 7. Enthalpy versus entropy for WT-OccK1, OccK1 ΔL3, and OccK1 ΔL4. The compensation temperature, T_c, was 299 ± 2 K. The free energy constant, ΔG_c°, was −2.31 ± 0.58 kJ/mol. The right axis shows the free energy, ΔG°, which was calculated at a temperature of 25 °C (open squares). The horizontal line is the weighted average of the equilibrium free energy ΔG° = −2.3 kJ/mol, which was determined at a temperature of 25 °C. Other conditions are similar to those presented in the legend of Figure 3.

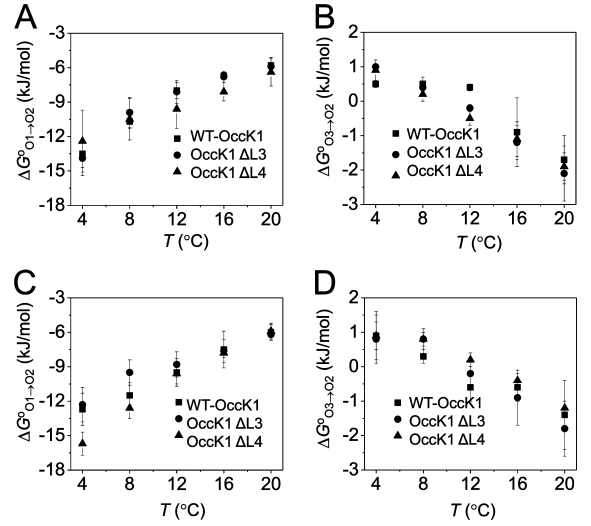

Figure 8. Free energies of the O_1 to O_2 and O_3 to O_2 current fluctuations, which were calculated at 25 °C. (A) $\Delta G_{O1\rightarrow O2}^{\circ}$ at a transmembrane potential of +40 mV. (B) $\Delta G_{O3\rightarrow O2}^{\circ}$ at a transmembrane potential of +40 mV. (C) $\Delta G_{O1\rightarrow O2}^{\circ}$ at a transmembrane potential of −40 mV. (A) $\Delta G_{O3\rightarrow O2}^{\circ}$ at a transmembrane potential of −40 mV. Other conditions are similar to those presented in the legend of Figure 3.

the $O_1 \rightarrow O_2$ and $O_3 \rightarrow O_2$ transitions on temperature. Because we inspected a relatively small temperature interval, we assumed that ΔH° and ΔS° are fairly temperature-independent. If so, ΔG° would change linearly with temperature, either increasing or decreasing.[47] This trend depends on the sign of ΔS°. Figure 8 shows that $\Delta G_{O1\rightarrow O2}^{\circ}$ is negative but increases by increasing temperature (Supporting Information, Table S5). That means that $\Delta H_{O1\rightarrow O2}^{\circ}$ and $\Delta S_{O1\rightarrow O2}^{\circ}$ are negative. On the contrary, we determined that $\Delta G_{O3\rightarrow O2}^{\circ}$ decreases by increasing temperature, indicating that $\Delta H_{O1\rightarrow O2}^{\circ}$ and $\Delta S_{O1\rightarrow O2}^{\circ}$ are positive. Such a finding suggests that the nature of both reversible transitions is different.

DISCUSSION

Existence of Diverse Thermally Activated Current Fluctuations within a Protein Nanopore. This detailed experimentation enabled the calculation of the alterations in enthalpic and entropic contributions to the kinetic rate constants of the transitions occurring among the three open substates. Changes in the quasithermodynamic quantities contributing to the two energetic barriers, leading to the transitions $O_2 \rightarrow O_1$, $O_1 \rightarrow O_2$, $O_2 \rightarrow O_3$, and $O_3 \rightarrow O_2$, are displayed in Table 1. These are the differential activation enthalpies ($\Delta\Delta H_{OccK1\text{-}mut}^{\ddagger}$), entropies ($\Delta\Delta S_{OccK1\text{-}mut}^{\ddagger}$), and free energies ($\Delta\Delta G_{OccK1\text{-}mut}^{\ddagger}$), which reflect alterations in the activation enthalpies, entropies, and free energies, respectively. They are resulted from local structural reorganizations owing to the two specific loop-deletion mutations, ΔL3 and ΔL4, as follows:

dx.doi.org/10.1021/cb5008025 | ACS Chem. Biol. 2015, 10, 784−794

Table 1. Differential Activation Free Enthalpies, Entropies, and Free Energies of OccK1 ΔL3 and OccK1 ΔL4

parameter	transmembrane potential (mV)	nanopore	$O_2 \rightarrow O_1$	$O_1 \rightarrow O_2$	$O_2 \rightarrow O_3$	$O_3 \rightarrow O_2$
$\Delta\Delta H_{OccK1\text{-}mut}^{\#}$ (kJ/mol)	+40	OccK1 ΔL3	16 ± 8	15 ± 1	0 ± 1	19 ± 3
		OccK1 ΔL4	−24 ± 7	25 ± 3	10 ± 6	25 ± 6
	−40	OccK1 ΔL3	−20 ± 2	5 ± 2	−3 ± 7	24 ± 9
		OccK1 ΔL4	60 ± 2	8 ± 3	5 ± 5	12 ± 5
$\Delta\Delta S_{OccK1\text{-}mut}^{\#}$ (J/mol K)	+40	OccK1 ΔL3	64 ± 22	54 ± 8	−6 ± 5	70 ± 12
		OccK1 ΔL4	−83 ± 16	92 ± 17	30 ± 19	70 ± 23
	−40	OccK1 ΔL3	−53 ± 10	13 ± 10	−13 ± 23	80 ± 15
		OccK1 ΔL4	210 ± 8	28 ± 6	16 ± 20	41 ± 3
$\Delta\Delta G_{OccK1\text{-}mut}^{\#\,a}$ (kJ/mol)	+40	OccK1 ΔL3	−3.1 ± 0.5	−1.1 ± 1.4	1.8 ± 0.5	−1.9 ± 0.6
		OccK1 ΔL4	0.7 ± 2.2	−2.4 ± 2.1	1.1 ± 0.3	−4.1 ± 2.4
	−40	OccK1 ΔL3	−4.2 ± 1.0	1.1 ± 1.0	1.0 ± 0.1	0.2 ± 1.5
		OccK1 ΔL4	−2.6 ± 0.4	−0.3 ± 1.2	0.2 ± 1.0	−0.2 ± 1.1

[a] $\Delta\Delta G_{OccK1\text{-}mut}^{\#}$ was calculated at a temperature of 25 °C.

$$\Delta\Delta H^{\ddagger}_{OccK1-mut} = \Delta H^{\ddagger}_{OccK1-mut} - \Delta H^{\ddagger}_{WT-OccK1}$$
$$\Delta\Delta S^{\ddagger}_{OccK1-mut} = \Delta S^{\ddagger}_{OccK1-mut} - \Delta S^{\ddagger}_{WT-OccK1}$$
$$\Delta\Delta G^{\ddagger}_{OccK1-mut} = \Delta\Delta H^{\ddagger}_{OccK1-mut} - T\Delta\Delta S^{\ddagger}_{WT-OccK1} \quad (12)$$

where the subscripts OccK1-mut and WT-OccK1 indicate the loop-deletion mutated and wild-type OccK1 protein nanopores, respectively.

One immediate observation is that the values of $\Delta\Delta G_{OccK1\text{-}mut}^{\ddagger}$ are relatively low, on the order of a few kilojoules per mole at 25 °C. This finding reinforces the fact that the local loop deletions, by producing modest alterations in the activation free energies, did not move the system away from equilibrium. On the contrary, a broad range of differential activation enthalpies and entropies was determined, revealing that the local conformational alterations in the loop packing were accompanied by major reconversions of the quasithermodynamic profile. In case of the transitions leading to the most probable open substate O_2, $\Delta\Delta H_{OccK1\text{-}mut}^{\ddagger}$ has positive values, which are favored by increased differential activation entropies $\Delta\Delta S_{OccK1\text{-}mut}^{\ddagger}$. If this result is coupled with small changes in $\Delta\Delta G_{OccK1\text{-}mut}^{\ddagger}$, the $O_1 \rightarrow O_2$ and $O_3 \rightarrow O_2$ transitions are likely impacted by a more loosely packed configuration of the loops in the most probable O_2 open substate. In other words, the removal of key electrostatic interactions encompassing both OccK1 ΔL3 and OccK1 ΔL4 was accompanied by a local increase in the loop flexibility at an enthalpic expense in the O_2 open substate. Table 1 also reveals significant changes of these differential quasithermodynamic parameters as a result of switching the polarity of the applied transmembrane potential, confirming the importance of local electric field on the electrostatic interactions underlying single-molecule conformational transitions in protein nanopores. For example, the differential activation enthalpy of OccK1 ΔL4 for the $O_2 \rightarrow O_1$ transition was −24 ± 7 kJ/mol at a transmembrane potential of +40 mV, but 60 ± 2 kJ/mol at an applied potential of −40 mV. These reversed enthalpic alterations corresponded to significant changes in the differential activation entropies from −83 ± 16 J/mol·K at +40 mV to 210 ± 8 J/mol·K at −40 mV.

Are Some Kinetic Rate Constants Slower at Elevated Temperatures? One counterintuitive observation was the temperature dependence of the kinetic rate constant $k_{O1\rightarrow O2}$ (Figure 5). In contrast to the other three rate constants, $k_{O1\rightarrow O2}$ decreased at higher temperatures. This result was unexpected, because the extracellular loops move faster at an elevated temperature, so that they take less time to transit back to where they were near the equilibrium position. Hence, the respective kinetic rate constant is increased. In other words, the kinetic barriers are expected to decrease by increasing temperature, which is in accord with the second law of thermodynamics. The only way for a deviation from this rule is that in which the ground energy level of a particular transition of the protein undergoes large temperature-induced alterations, so that the system remains for a longer duration in a trapped open substate.[48] It is likely that the molecular nature of the interactions underlying such a trapped substate involves complex dynamics of solvation-desolvation forces that lead to stronger hydrophobic contacts at elevated temperatures, so that the protein loses flexibility by increasing temperature. This is the reason for the origin of the negative activation enthalpies, which are often noticed in protein folding kinetics.[49,50] In our situation, the source of this abnormality is the negative activation enthalpy of the $O_1 \rightarrow O_2$ transition, which is strongly compensated by a substantial reduction in the activation entropy,[49] suggesting the local formation of new intramolecular interactions that accompany the transition process. Under specific experimental contexts, the overall activation enthalpy of a certain transition can become negative, at least in part owing to transient dissociations of water molecules from the protein side chains and backbone, favoring strong hydrophobic interactions. Taken together, these interactions do not violate the second law of thermodynamics.

Enthalpy−Entropy Compensation. Enthalpy−entropy compensation is a ubiquitous and unquestionable phenomenon,[44,45,51−54] which is based upon basic thermodynamic arguments. In simple terms, if a conformational perturbation of a biomolecular system is characterized by an increase (or a decrease) in the equilibrium enthalpy, then this is also accompanied by an increase (or a decrease) in the equilibrium entropy. Under experimental circumstances at thermodynamic equilibrium between two open substates, the standard free energy ΔG° must be very small.[55] Otherwise, the biomolecular system would depart from equilibrium, so that a direct quantitative comparison among the kinetics of the three protein nanopores, WT-OccK1, OccK1 ΔL3, and OccK1 ΔL4, would not be meaningful. Here, we have determined that indeed the weighted average of ΔG° was −2.3 kJ/mol. In this way, it is conceivable that a large enthalpic modification associated with each reversible transition is accompanied by a large entropic alteration, thanks to the standard thermodynamic relation $\Delta G^{\circ} = \Delta H^{\circ} - T\Delta S^{\circ}$. Therefore, enthalpy−entropy

dx.doi.org/10.1021/cb5008025 | ACS Chem. Biol. 2015, 10, 784−794

compensation is not in conflict in any way with equilibrium thermodynamic formalisms. We are aware that using van't Hoff plots to determine the linear relationship between $\Delta H^{\ddagger}$ and $\Delta S^{\ddagger}$, especially if the temperature range of the collected data is small, is prone to some statistical errors. For example, Sharp showed that if the compensating temperature, T_c, lies within 20% of the average experimental temperature, T_{av}, the $\Delta H - \Delta S$ linear correlation is unlikely to be statistically significant.[56] Indeed, if our average experimental temperature was T_{av} = 286 K and T_c = 300 K, then the above-mentioned condition is met, so that we interpret that a linearity relationship between $\Delta H^{\ddagger}$ and $\Delta S^{\ddagger}$ was likely impacted by statistical correlation errors. The physical origin of the compensating nature of enthalpy and entropy is not clear, as several competing models have been proposed. One postulation has been that of the solvent reorganization during the reversible transitions that accompany all chemical reactions,[57,58] ligand-binding protein complex formation,[23,52,53,59] and protein folding−unfolding transitions.[60−62] Grunwald and Steel have shown that all of these processes undergo major changes in the activation enthalpies and entropies, involving hydrogen bonding-directed solvation.[57] Since the overall change in the free energy for solvent reorganization is zero according to the second law of thermodynamics, then the enthalpy−entropy compensation is valid within these systems, providing a linear relationship between ΔH° and ΔS°, whose slope, T_c, is near to the experimental temperature.[54]

Temperature-Induced Changes in the Free Energies Are Greater than the Voltage-Induced Alterations of the Same Energetic Quantities. Temperature effect was always greater than the voltage effect. Because $\Delta G_{O3\rightarrow O2}^{\circ}$ is positive at temperatures smaller than 4 °C, the most probable open substate was O_3 under such low-temperature contexts. This conclusion was not impacted by the sign switch of the applied transmembrane potential, confirming the voltage-dependent symmetry of the gating energetics of β-barrel membrane proteins.[12] This is in contrast to the asymmetric voltage-dependent gating energetics displayed by protein channels made from bundles of α helices.[63,64] Moreover, the temperature-induced changes in the free energies $\Delta G_{O1\rightarrow O2}^{\circ}$ and $\Delta G_{O3\rightarrow O2}^{\circ}$ were always greater than the voltage-induced alterations of the same energetic quantities. For example, changing temperature within the interval 4 through 20 °C produced a modification on $\Delta G_{O1\rightarrow O2}^{\circ}$ of ∼7.7 kJ/mol in the case of WT-OccK1 (Figure 8A,C; Supporting Information, Table S5). On the contrary, changing the applied transmembrane potential over the range −80 through +80 mV produced an alteration on $\Delta G_{O1\rightarrow O2}^{\circ}$ of only ∼0.7 kJ/mol (Supporting Information, Figure S5). In addition, past single-channel examinations of OccK1 also revealed that the ionic strength-induced modifications in the free energies $\Delta G_{O1\rightarrow O2}^{\circ}$ and $\Delta G_{O3\rightarrow O2}^{\circ}$ were modest.[27] Thus, increasing the salt concentration in the chamber from 1 to 4 M, the alterations of the free energies were smaller than ∼2.5 kJ/mol. Taken together, we conclude that the effect of ionic strength and applied transmembrane potential on the energetics of gating fluctuations is small, as compared to the energetic effect of temperature.

Implications of This Approach in the Realm of Membrane Protein Design and Dynamics. Long-lived current fluctuations are generally directly observed and well-characterized by single-channel electrical recordings.[65] However, under many experimental contexts, the average duration of conformational fluctuations are well below the time resolution limit of experimental setup. A complete understanding of the presence of these hidden substates is essential for a mechanistic understanding of the overall dynamics of a membrane protein nanopore. Therefore, recent advances in electronics,[66] allowing the direct detection of current fluctuations at submicrosecond resolution, will likely enable unraveling the detailed energetic landscape of the dynamics of single protein nanopores. Moreover, developments in the single-channel recording analysis demonstrated that the current fluctuations among various conductive substates reflect subtle changes in the channel length and cross-sectional area of the pore interior. Robertson and colleagues, using single-molecule mass spectrometry, have identified subangstrom resolution of geometrical changes associated with various current transitions.[67] This methodology is critically important, because it shows profound implications for both structural and temporal alterations accompanying a given conformational transition of a fluctuating protein nanopore.

CONCLUSIONS

In summary, we pursued a systematic determination of the quasithermodynamic contributions to a fluctuating protein nanopore. Targeted loop-deletion alterations, which line the central constriction of this protein nanopore, produced modest changes in the differential activation free energies, in the range near the thermal energy but substantial modifications of the differential activation enthalpies and entropies. Because these protein derivatives produced significant changes in the kinetics of the single-channel electrical recordings, we conclude that L3 and L4 indeed contribute to the mechanisms of gating fluctuations of OccK1.[20,21] Moreover, changes of the equilibrium gating transitions of OccK1 were directly determined without the need for fluorescent labeling of the fluctuating part of this protein nanopore. The compensatory nature of the quasithermodynamic contributions to the kinetic rate constants can be interpreted in terms of local conformational alterations of the loop packing and flexibility, which is reflected by enthalpic−entropic reconfigurations of the interactions driving these directly determined current fluctuations.

METHODS

Cloning, Overexpression, and Purification of Native WT-OccK1 and Its Derivatives. The *occk1* gene, without the segment encoding the signal sequence, was amplified from genomic DNA of *P. aeruginosa* and cloned into the pB22 vector.[68] At the N-terminus, this gene construct contained segments encoding the *E. coli YtfM* signal sequence, a seven-histidine tag (His tag), and a TEV protease cleavage site for the His tag removal. The derivatives of the OccK1 protein were produced by PCR (Expand high fidelity PCR system; Roche, Table S2). All OccK1 proteins were expressed in C43 (DE3) *E. coli* cells. Other details of the protocols for the protein overexpression and purification used in this study were reported in a prior publication.[27] The purity of the OccK1 protein samples was determined by standard SDS-PAGE gel electrophoresis (Supporting Information, Figure S2).

Single-Channel Current Recordings. Single-channel current measurements were conducted using planar lipid membranes.[29,69] Both chambers of the bilayer apparatus were separated by a Teflon partition (Goodfellow Corporation), whose thickness was 25 μm. An 80-μm-diameter aperture in the septum was pretreated with hexadecane (Aldrich Chemical Co.), which was dissolved in highly purified *n*-pentane (Burdick and Jackson) at a concentration of 10% (v/v). The bilayer was generated using 1,2-diphytanoyl-*sn*-glycerophosphocholine (Avanti Polar Lipids Inc.). The standard electrolyte

dx.doi.org/10.1021/cb5008025 | ACS Chem. Biol. 2015, 10, 784−794

in both chambers was 2000 mM KCl, 10 mM potassium phosphate, pH 7.4. Potassium phosphate was employed owing to its exceptional low temperature coefficient.[70] The OccK1 proteins were added to the *cis* chamber, which was at ground. Single-channel currents were collected by using an Axopatch 200B patch-clamp amplifier (Molecular Devices) attached to the bilayer chamber by Ag/AgCl electrodes.[5,71] A Desktop computer (Dell) equipped with a Digitdata 1440 A/D converter (Molecular Devices) was employed for single-channel data collection. Electrical traces were filtered by an eight-pole low-pass Bessel filter (Model 900, Frequency Devices) at a corner frequency of 10 kHz and recorded at a frequency of 50 kHz. For the data acquisition and analysis, we used pClamp 10.2 software (Molecular Devices). The temperature-control experiments were carried out using a Dagan HCC-100A controller (Dagan Corporation). Other details of the approach involving reconstituted planar lipid bilayers for the temperature dependence of single-channel currents were published previously.[24,25,28]

Molecular Modeling. The molecular model of OccK1 was created by using the Chimera software package[72] as well as the Protein Data Bank entry code 2qtk.pdb.[15]

■ ASSOCIATED CONTENT

Supporting Information

(i) Top view of the molecular surface of eight members of the outer membrane carboxylate channel (Occ) family of *P. aeruginosa*. (ii) The SDS-PAGE gel analysis of the purified *P. aeruginosa* OccK channels. (iii) Distribution of single-channel electrical conductance of the members of the Occ family. (iv) The biophysical features of the extracellular loops of the WT-OccK1 protein. (v) The biophysical characteristics of two loop-deletion mutants of OccK1. (vi) Dependence of the substate conductance (O_1, O_2, O_3) on the KCl concentration. (vii) Determination of the upper limits of the single-channel conductance of the OccK1 protein nanopore inferred from KCl saturation curves. (viii) Enthalpic and entropic contributions to single-channel current fluctuations of the WT-OccK1, OccK1 ΔL3, and OccK1 ΔL4 protein nanopores. (ix) Tabular data of the temperature dependence of the standard free energies $\Delta G_{O1\rightarrow O2}^{\circ}$ and $\Delta G_{O3\rightarrow O2}^{\circ}$. (x) Dependence of the equilibrium free energies $\Delta G_{O1\rightarrow O2}^{\circ}$ and $\Delta G_{O1\rightarrow O2}^{\circ}$, which were determined at 25 °C, on the applied transmembrane potential. These materials are available free of charge via the Internet at http://pubs.acs.org.

■ AUTHOR INFORMATION

Corresponding Author

*Phone: 315-443-8078. Fax: 315-443-9103. E-mail: lmovilea@syr.edu.

Author Contributions

B.R.C. performed experiments and conducted data analysis; B.v.d.B. and L.M. designed research; L.M. wrote the paper.

Notes

The authors declare no competing financial interest.

■ ACKNOWLEDGMENTS

We thank our co-workers in the Movileanu and van den Berg research groups for stimulating discussions. We are also grateful to Eric Schiff and Arthur Yelon for introducing us to the area of enthalpy−entropy compensation as well as constructive discussions at an earlier phase of this article. This paper was funded in part by the National Institutes of Health (R01 GM088403, L.M.; R01 GM085785, B.v.d.B.).

■ REFERENCES

(1) Kullman, L., Gurnev, P. A., Winterhalter, M., and Bezrukov, S. M. (2006) Functional subconformations in protein folding: evidence from single-channel experiments. *Phys. Rev. Lett. 96*, 038101.

(2) Hong, H., Szabo, G., and Tamm, L. K. (2006) Electrostatic couplings in OmpA ion-channel gating suggest a mechanism for pore opening. *Nat. Chem. Biol. 2*, 627−635.

(3) Hwang, W. L., Chen, M., Cronin, B., Holden, M. A., and Bayley, H. (2008) Asymmetric droplet interface bilayers. *J. Am. Chem. Soc. 130*, 5878−5879.

(4) Mohammad, M. M., and Movileanu, L. (2010) Impact of distant charge reversals within a robust beta-barrel protein pore. *J. Phys. Chem. B 114*, 8750−8759.

(5) Mohammad, M. M., Howard, K. R., and Movileanu, L. (2011) Redesign of a plugged beta-barrel membrane protein. *J. Biol. Chem. 286*, 8000−8013.

(6) Volkan, E., Kalas, V., Pinkner, J. S., Dodson, K. W., Henderson, N. S., Pham, T., Waksman, G., Delcour, A. H., Thanassi, D. G., and Hultgren, S. J. (2013) Molecular basis of usher pore gating in Escherichia coli pilus biogenesis. *Proc. Natl. Acad. Sci. U. S. A. 110*, 20741−20746.

(7) Chen, M., Khalid, S., Sansom, M. S., and Bayley, H. (2008) Outer membrane protein G: Engineering a quiet pore for biosensing. *Proc. Natl. Acad. Sci. U. S. A. 105*, 6272−6277.

(8) Zhuang, T., and Tamm, L. K. (2014) Control of the Conductance of Engineered Protein Nanopores through Concerted Loop Motions. *Angew. Chem., Int. Ed. Engl. 53*, 5897−5902.

(9) Movileanu, L. (2008) Squeezing a single polypeptide through a nanopore. *Soft Matter 4*, 925−931.

(10) Movileanu, L. (2009) Interrogating single proteins through nanopores: challenges and opportunities. *Trends Biotechnol. 27*, 333−341.

(11) Qian, H. (2002) From discrete protein kinetics to continuous Brownian dynamics: a new perspective. *Protein Sci. 11*, 1−5.

(12) Bainbridge, G., Gokce, I., and Lakey, J. H. (1998) Voltage gating is a fundamental feature of porin and toxin beta-barrel membrane channels. *FEBS Lett. 431*, 305−308.

(13) Bainbridge, G., Mobasheri, H., Armstrong, G. A., Lea, E. J. A., and Lakey, J. H. (1998) Voltage-gating of Escherichia coli porin: A cystine-scanning mutagenesis study of loop 3. *J. Mol. Biol. 275*, 171−176.

(14) Mapingire, O. S., Henderson, N. S., Duret, G., Thanassi, D. G., and Delcour, A. H. (2009) Modulating effects of the plug, helix, and N- and C-terminal domains on channel properties of the PapC usher. *J. Biol. Chem. 284*, 36324−36333.

(15) Biswas, S., Mohammad, M. M., Movileanu, L., and van den Berg, B. (2008) Crystal structure of the outer membrane protein OpdK from Pseudomonas aeruginosa. *Structure 16*, 1027−1035.

(16) Biswas, S., Mohammad, M. M., Patel, D. R., Movileanu, L., and van den Berg, B. (2007) Structural insight into OprD substrate specificity. *Nat. Struct. Mol. Biol. 14*, 1108−1109.

(17) Liu, J., Eren, E., Vijayaraghavan, J., Cheneke, B. R., Indic, M., van den Berg, B., and Movileanu, L. (2012) OccK Channels from Pseudomonas aeruginosa Exhibit Diverse Single-channel Electrical Signatures, but Conserved Anion Selectivity. *Biochemistry 51*, 2319−2330.

(18) Liu, J., Wolfe, A. J., Eren, E., Vijayaraghavan, J., Indic, M., van den Berg, B., and Movileanu, L. (2012) Cation Selectivity is a Conserved Feature in the OccD Subfamily of Pseudomonas aeruginosa. *Biochim. Biophys. Acta. Biomembr. 1818*, 2908−2916.

(19) Hancock, R. E. W., and Tamber, S. (2004) Porins of the Outer Membrane of Pseudomonas aeruginosa, In *Bacterial and Eukaryotic Porins: Structure, Function, Mechanism* (Benz, R., Ed.), pp 61−77, Wiley-VCH, Weinheim, Germany.

(20) Eren, E., Parkin, J., Adelanwa, A., Cheneke, B. R., Movileanu, L., Khalid, S., and van den Berg, B. (2013) Towards understanding the outer membrane uptake of small molecules by *Pseudomonas aeruginosa*. *J. Biol. Chem. 288*, 12042−12053.

(21) Eren, E., Vijayaraghavan, J., Liu, J., Cheneke, B. R., Touw, D. S., Lepore, B. W., Indic, M., Movileanu, L., and van den Berg, B. (2012) Substrate specificity within a family of outer membrane carboxylate channels. *PLoS Biology 10*, e1001242.
(22) Howorka, S., Movileanu, L., Braha, O., and Bayley, H. (2001) Kinetics of duplex formation for individual DNA strands within a single protein nanopore. *Proc. Natl. Acad. Sci. U. S. A. 98*, 12996–13001.
(23) Kang, X. F., Gu, L. Q., Cheley, S., and Bayley, H. (2005) Single Protein Pores Containing Molecular Adapters at High Temperatures. *Angew. Chem., Int. Ed. Engl. 44*, 1495–1499.
(24) Jung, Y., Bayley, H., and Movileanu, L. (2006) Temperature-responsive protein pores. *J. Am. Chem. Soc. 128*, 15332–15340.
(25) Mohammad, M. M., and Movileanu, L. (2008) Excursion of a single polypeptide into a protein pore: simple physics, but complicated biology. *Eur. Biophys. J. 37*, 913–925.
(26) Chimerel, C., Movileanu, L., Pezeshki, S., Winterhalter, M., and Kleinekathofer, U. (2008) Transport at the nanoscale: Temperature dependence of ion conductance. *Eur. Biophys. J. 38*, 121–125.
(27) Cheneke, B. R., van den Berg, B., and Movileanu, L. (2011) Analysis of gating transitions among the three major open states of the OpdK channel. *Biochemistry 50*, 4987–4997.
(28) Cheneke, B. R., Indic, M., van den Berg, B., and Movileanu, L. (2012) An Outer Membrane Protein undergoes Enthalpy- and Entropy-driven Transitions. *Biochemistry 51*, 5348–5358.
(29) Mohammad, M. M., Iyer, R., Howard, K. R., McPike, M. P., Borer, P. N., and Movileanu, L. (2012) Engineering a Rigid Protein Tunnel for Biomolecular Detection. *J. Am. Chem. Soc. 134*, 9521–9531.
(30) Yamashita, E., Zhalnina, M. V., Zakharov, S. D., Sharma, O., and Cramer, W. A. (2008) Crystal structures of the OmpF porin: function in a colicin translocon. *EMBO J. 27*, 2171–2180.
(31) Cramer, W. A., Zakharov, S. D., Saif, H. S., Zhang, H., Baniulis, D., Zhalnina, M. V., Soriano, G. M., Sharma, O., Rochet, J. C., Ryan, C., Whitelegge, J., Kurisu, G., and Yamashita, E. (2011) Membrane proteins in four acts: Function precedes structure determination. *Methods 55*, 415–420.
(32) Basle, A., Rummel, G., Storici, P., Rosenbusch, J. P., and Schirmer, T. (2006) Crystal structure of osmoporin OmpC from E. coli at 2.0 A. *J. Mol. Biol. 362*, 933–942.
(33) McManus, O. B., and Magleby, K. L. (1988) Kinetic states and modes of single large-conductance calcium-activated potassium channels in cultured rat skeletal-muscle. *J. Physiol. (London) 402*, 79–120.
(34) Movileanu, L., Cheley, S., and Bayley, H. (2003) Partitioning of individual flexible polymers into a nanoscopic protein pore. *Biophys. J. 85*, 897–910.
(35) Bikwemu, R., Wolfe, A. J., Xing, X., and Movileanu, L. (2010) Facilitated translocation of polypeptides through a single nanopore. *J. Phys.: Condens. Matter 22*, 454117.
(36) Colquhoun, D., and Sigworth, F. J. (1995) Fitting and statistical analysis of single-channel records, In *Single-channel recording*, 2nd ed., (Sackmann, B. N. E., Ed.), pp 483–587, Plenum Press, New York.
(37) Mortensen, M., and Smart, T. G. (2007) Single-channel recording of ligand-gated ion channels. *Nat. Protoc. 2*, 2826–2841.
(38) McManus, O. B., Blatz, A. L., and Magleby, K. L. (1987) Sampling, Log Binning, Fitting, and Plotting Durations of Open and Shut Intervals From Single Channels and the Effects of Noise. *Pflugers Arch. 410*, 530–553.
(39) Aidley, D. J., and Stanfield, P. R. (1996) *Ion channels - Molecules in action*, Cambridge University Press, Cambridge.
(40) Moss, G. W. J., and Moczydlowski, E. (2002) Concepts of single-channel analysis: inferring function from fluctuations, In *Ion Channels - A Practical Approach*, Second ed., (Ashley, R. H., Ed.), pp 69–112, Oxford University Press, Oxford.
(41) Hanggi, P., Talkner, P., and Borkovec, M. (1990) Reaction-Rate Theory - 50 Years After Kramers. *Rev. Mod. Phys. 62*, 251–341.
(42) Andersen, O. S. (1999) Graphic representation of the results of kinetic analyses. *J. Gen. Physiol. 114*, 589–590.
(43) Starikov, E. B., and Norden, B. (2012) Entropy-enthalpy compensation as a fundamental concept and analysis tool for systematical experimental data. *Chem. Phys. Lett. 538*, 118–120.
(44) Starikov, E. B., and Norden, B. (2012) Entropy-enthalpy compensation may be a useful interpretation tool for complex systems like protein-DNA complexes: An appeal to experimentalists. *Appl. Phys. Lett. 100*, 193701.
(45) Movileanu, L., and Schiff, E. A. (2013) Entropy-enthalpy Compensation of Biomolecular Systems in Aqueous Phase: a Dry Perspective. *Monatsh. Chem. 144*, 59–65.
(46) Movileanu, L., Benevides, J. M., and Thomas, G. J. (2002) Determination of base and backbone contributions to the thermodynamics of premelting and melting transitions in B DNA. *Nucleic Acids Res. 30*, 3767–3777.
(47) Clapham, D. E., and Miller, C. (2011) A thermodynamic framework for understanding temperature sensing by transient receptor potential (TRP) channels. *Proc. Natl. Acad. Sci. U. S. A 108*, 19492–19497.
(48) Oliveberg, M., Tan, Y. J., and Fersht, A. R. (1995) Negative activation enthalpies in the kinetics of protein folding. *Proc. Natl. Acad. Sci. U. S. A 92*, 8926–8929.
(49) Marchal, S., Font, J., Ribo, M., Vilanova, M., Phillips, R. S., Lange, R., and Torrent, J. (2009) Asymmetric kinetics of protein structural changes. *Acc. Chem. Res. 42*, 778–787.
(50) Noronha, M., Gerbelova, H., Faria, T. Q., Lund, D. N., Smith, D. A., Santos, H., and Macanita, A. L. (2010) Thermal unfolding kinetics of ubiquitin in the microsecond-to-second time range probed by Tyr-59 fluorescence. *J. Phys. Chem. B 114*, 9912–9919.
(51) Wilfong, E. M., Kogiso, Y., Muthukrishnan, S., Kowatz, T., Du, Y., Bowie, A., Naismith, J. H., Hadad, C. M., Toone, E. J., and Gustafson, T. L. (2011) A multidisciplinary approach to probing enthalpy-entropy compensation and the interfacial mobility model. *J. Am. Chem. Soc. 133*, 11515–11523.
(52) Fenley, A. T., Muddana, H. S., and Gilson, M. K. (2012) Entropy-enthalpy transduction caused by conformational shifts can obscure the forces driving protein-ligand binding. *Proc. Natl. Acad. Sci. U. S. A 109*, 20006–20011.
(53) Ferrante, A., and Gorski, J. (2012) Enthalpy-entropy compensation and cooperativity as thermodynamic epiphenomena of structural flexibility in ligand-receptor interactions. *J. Mol. Biol. 417*, 454–467.
(54) Chodera, J. D., and Mobley, D. L. (2013) Entropy-enthalpy compensation: role and ramifications in biomolecular ligand recognition and design. *Annu. Rev. Biophys. 42*, 121–142.
(55) Qian, H. (1998) Entropy-enthalpy compensation: Conformational fluctuation and induced-fit. *J. Chem. Phys. 109*, 10015–10017.
(56) Sharp, K. (2001) Entropy-enthalpy compensation: fact or artifact? *Protein Sci. 10*, 661–667.
(57) Grunwald, E., and Steel, C. (1995) Solvent Reorganization and Thermodynamic Enthalpy-Entropy Compensation. *J. Am. Chem. Soc. 117*, 5687–5692.
(58) Breiten, B., Lockett, M. R., Sherman, W., Fujita, S., Al-Sayah, M., Lange, H., Bowers, C. M., Heroux, A., Krilov, G., and Whitesides, G. M. (2013) Water networks contribute to enthalpy/entropy compensation in protein-ligand binding. *J. Am. Chem. Soc. 135*, 15579–15584.
(59) Whitesides, G. M., and Krishnamurthy, V. M. (2005) Designing ligands to bind proteins. *Q. Rev. Biophys. 38*, 385–395.
(60) Liu, Z., and Chan, H. S. (2005) Desolvation is a likely origin of robust enthalpic barriers to protein folding. *J. Mol. Biol. 349*, 872–889.
(61) Nickson, A. A., Stoll, K. E., and Clarke, J. (2008) Folding of a LysM domain: entropy-enthalpy compensation in the transition state of an ideal two-state folder. *J. Mol. Biol. 380*, 557–569.
(62) Forrey, C., Douglas, J. F., and Gilson, M. K. (2012) The Fundamental Role of Flexibility on the Strength of Molecular Binding. *Soft. Matter 8*, 6385–6392.
(63) Gupta, S., and Auerbach, A. (2011) Temperature dependence of acetylcholine receptor channels activated by different agonists. *Biophys. J. 100*, 895–903.

(64) Gupta, S., and Auerbach, A. (2011) Mapping heat exchange in an allosteric protein. *Biophys. J. 100*, 904−911.
(65) Sackmann, B., and Neher, E. (1995) *Single-Channel Recording*, Second ed., Kluwer Academic/Plenum Publishers, New York.
(66) Rosenstein, J. K., Wanunu, M., Merchant, C. A., Drndic, M., and Shepard, K. L. (2012) Integrated nanopore sensing platform with sub-microsecond temporal resolution. *Nat. Methods 9*, 487−492.
(67) Robertson, J. W., Kasianowicz, J. J., and Reiner, J. E. (2010) Changes in ion channel geometry resolved to sub-angstrom precision via single molecule mass spectrometry. *J. Phys.: Condens. Matter 22*, 454108.
(68) Guzman, L. M., Belin, D., Carson, M. J., and Beckwith, J. (1995) Tight regulation, modulation, and high-level expression by vectors containing the arabinose PBAD promotor. *J. Bacteriol. 177*, 4121−4130.
(69) Niedzwiecki, D. J., Mohammad, M. M., and Movileanu, L. (2012) Inspection of the Engineered FhuA deltaC/delta4L Protein Nanopore by Polymer Exclusion. *Biophys. J. 103*, 2115−2124.
(70) Dawson, R. M. C., Elliot, D. C., Elliot, W. H., Jones, K. M. (1986) *Data for biochemical research*, Clarendon Press, Oxford.
(71) Niedzwiecki, D. J., Iyer, R., Borer, P. N., and Movileanu, L. (2013) Sampling a Biomarker of the Human Immunodeficiency Virus across a Synthetic Nanopore. *ACS Nano 7*, 3341−3350.
(72) Pettersen, E. F., Goddard, T. D., Huang, C. C., Couch, G. S., Greenblatt, D. M., Meng, E. C., and Ferrin, T. E. (2004) UCSF Chimera–a visualization system for exploratory research and analysis. *J. Comput. Chem. 25*, 1605−1612.